Hindawi
Mathematical Problems in Engineering
Volume 2022, Article ID 3381003, 10 pages
https://doi.org/10.1155/2022/3381003

Research Article

Uncertainty in the Stability for Excavated Surface during the Cutter Replacement in Tunneling Construction

Shiguang Chen,[1] Hai Li,[1] Juchuan He,[1] Zhongwei Li,[2] Jin Tao,[2] and Qian Zhai[2]

[1]*China Construction Eighth Engineering Division Rail Transit Construction Co., LTD, Nanjing 210000, Jiangsu, China*
[2]*Bridge Engineering Research Center of Southeast University, School of Civil Engineering, Southeast University, Nanjing, Jiangsu 210008, China*

Correspondence should be addressed to Qian Zhai; 101012332@seu.edu.cn

Received 25 November 2021; Revised 26 January 2022; Accepted 4 February 2022; Published 8 March 2022

Academic Editor: A. M. Bastos Pereira

In the process of tunnel excavation, the cutter wear rate is accelerated when the tunnel boring machine (TBM) passes through the rock stratum and the cutter is commonly replaced frequently during the excavation. In the replacement stage, the stability of the excavation surface is crucial to the operation of the project. In this study, commercial software PLAXIS3D is adopted for the evaluation of the stability of the excavation surface by considering different scenarios. The Hoek–Brown failure criterion is adopted as the constitutive model for the rock in the numerical analysis. Various failure modes under different working conditions are obtained. The results from the numerical analyses indicate that the excavation surface during the replacement is stable for those different scenarios. The factor of safety (FoS) for the stability of the excavation surface varies from 2.88 to 14.04. The failure modes near the excavation surface can be divided into four types: (i) central inward invasion, (ii) bilateral inward invasion, (iii) sliding, and (iv) outward invasion. With the increase of support pressure, the safety factor increases first and then decreases.

1. Introduction

It is known that the geotechnical problems are commonly associated with shear failure of soil or rock. As a result, most of the stability evaluations for the geotechnical problems are based on the failure criterion of soil or rock. The shear strength reduction method is commonly adopted by the numerical analysis and has received most attention in geotechnical engineering [1, 2]. Dyson and Tolooiyan [3] and P. Li et al. [4] conducted the numerical analysis for the excavation work by adopting the shear strength reduction method. Lu et al. [5] and Shi et al. [6] adopted the shear strength reduction method to calculate the stability of excavation surface in the tunnel construction. Fu and Liao [7] and You et al. [8] incorporated the Hoek–Brown failure criterion of rock into the shear strength reduction method in the evaluation of the stability for the rock slope.

The cutter of TBM is commonly replaced frequently in the tunnel excavation. The stability of the excavation surface is crucial to the operation during the replacement of the cutter. In this paper, numerical analyses are conducted to evaluate the stability of the excavated rock surface by adopting the shear strength reduction method. The supporting pressures on the excavated weathered rock are computed by considering different working conditions. Subsequently, the failure modes of the excavated rock surface are categorized and discussed.

2. The Principles of the Shear Strength Reduction Method

Both principles of the shear strength reduction method incorporating Mohr–Coulomb and Hoek–Brown failure criteria are introduced in this section.

2.1. Shear Strength Reduction Method Incorporating the Mohr–Coulomb Failure Criterion. The Mohr–Coulomb failure criterion, as illustrated in (1) [9], is commonly

adopted as the constitutive model for the soil in the numerical analysis. The computed FoS is obtained by reducing the shear strength of soil until the soil becomes unstable. The shear strength of soil either in drained condition or undrained condition can be gradually decreased, as shown in (2) [10], until the FoS is obtained:

$$\tau = c' + (\sigma - u_w)\tan\phi', \tag{1}$$

where t is the shear strength of soil for the drained condition, c' is the effective cohesion, s is the normal stress, u_w is the pore-water pressure, and ϕ' is the effective internal friction angle.

$$\sum M_{sf} = \frac{\tan\phi_{input}}{\tan\phi_{reduced}} = \frac{c_{input}}{c_{reduced}} = \frac{s_{u,input}}{s_{u,reduced}}, \tag{2}$$

where the subscript *input* denotes the original shear strength parameter before the reduction, the subscript *reduced* denotes the shear strength parameter after the reduction, and ΣM_{sf} is the reduction multiple. The FoS is obtained by increasing the value of ΣM_{sf} until the instability occurs. In the reduction process, the strength of the structural elements such as plate, pile, and wall remains unchanged, and only soil parameters are reduced.

Hammah et al. [11] and Benz et al. [12] indicated that the strength of rock mass was nonlinear, and its failure envelope was inconsistent with the linear Mohr–Coulomb criterion. Especially, under high-stress condition, the strength characteristics of the rock surrounding the tunnel with respect to the strain show obvious nonlinearity. The Hoek–Brown failure criterion is a semiempirical model that can be used for the estimation of the shear strength of intact rock or jointed rock mass. It has become one of the most widely used guidelines in the field of strength prediction and stability analysis of rock masses by using the Hoek–Brown model due to its ability to better characterize the nonlinear failure of jointed rock masses [13, 14].

2.2. Strength Reduction Method Based on Hoek–Brown Criterion. Hoek–Brown criterion was proposed in 1980 as

$$\sigma_1' = \sigma_3' + \sigma_{ci}\left(m_b\frac{\sigma_3'}{\sigma_{ci}} + s\right)^a, \tag{3}$$

where σ_1' and σ_3' are the major and minor effective principle stresses at failure, σ_{ci} is the uniaxial compressive strength of the intact rock material, and m_b is the reduced value of the intact rock parameter m_i, which can be obtained by triaxial rock test or determined according to the rock type based on the reference value of literature [15, 16]:

$$m_b = m_i e^{(GSI-100/28-14D)}, \tag{4}$$

where D is the disturbance coefficient, which reflects the degree of rock blasting damage and stress release. The variation range of D is 0–1.0. D of undisturbed rock is 0 and D of strongly disturbed rock is 1.0. GSI stands for geological strength index, and its value ranges from 0 to 100. s and a are the material constants reflecting the joint and disturbance characteristics of rock mass that can be expressed as

$$\begin{aligned} s &= e^{(GSI-100/9-3D)}, \\ a &= 0.5 + \frac{1}{6}\left(e^{-(GSI/15)} - e^{-(20/3)}\right). \end{aligned} \tag{5}$$

Benz et al. [12] introduced ΣM_{sf} into the yield formula f_{HB} of the Hoek–Brown model by fitting the instantaneous friction angle and obtained FoS with the same meaning as that in the Mohr–Coulomb model:

$$\begin{aligned} f_{HB} &= \sigma_1' - \sigma_3' + \overline{f}_{red}(\sigma_3'), \\ \overline{f}_{red} &= \frac{\overline{f}}{\eta} \\ &= \frac{\sigma_{ci}}{\eta}\left(m_b\frac{-\sigma_3'}{\sigma_{ci}} + s\right)^a, \\ \eta &= \frac{1}{2}\left[\sum M_{sf}\left(2 - \overline{f'}\right)\sqrt{1 + \frac{\left(1/\sum M_{sf}^2 - 1\right)\overline{f'}^2}{\left(2 - \overline{f'}\right)^2}} + \overline{f'}\right], \\ \overline{f'} &= \frac{\partial\overline{f}}{\partial\sigma_3'}, \\ &= -am_b\left(m_b\frac{-\sigma_3'}{\sigma_{ci}} + s\right)^{a-1}, \end{aligned} \tag{6}$$

where η is the reduced strength factor, and other parameters are as described earlier.

The shear strength reduction multiple ΣM_{sf} with respect to the displacement of the characteristic point of the excavation surface is plotted, as shown Figure 1. With the increasing displacement of the characteristic point, ΣM_{sf} tends to a constant value, indicating the failure. Consequently, the obtained ΣM_{sf} represents the FoS for the stability of the excavated surface.

3. The Stress-Strain Analyses of the Tunnel Excavation Work

3.1. Introduction of the Tunneling Project. To connect the Xinjizhou and Binjiang water plant on the east bank of Yangtze River, the tunnel passing through the Yangtze River riverbed is under construction. The total length of the tunnel is 1945 m, runs from east to the west, with a maximum slope of 4.59%. The buried depth of the tunnel is around 10.77 to 51.53 m, and the maximum pore-water pressure is about 570 kPa. The geology of soil strata is found to be fluid plastic silty clay, silty clay mixed with silty soil, highly weathered diorite porphyrite, moderately weathered diorite porphyrite, and fine sand stratum, as shown in Figure 2.

3.2. Numerical Modeling. According to the construction sequence, there are total five chamber opening points for the replacement of the cutter. All of those opening points are located in moderately weathered diorite porphyrites. There

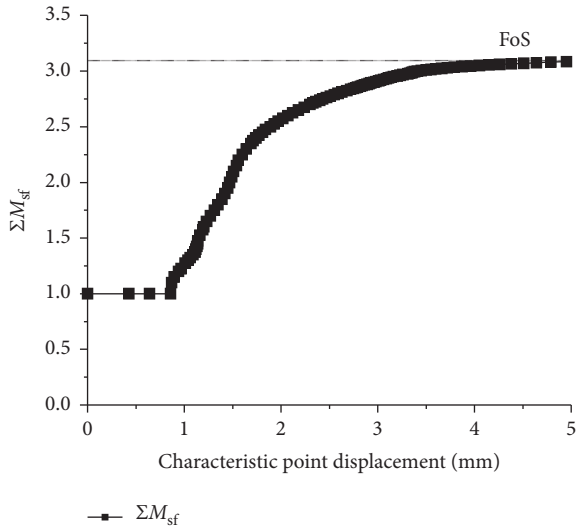

Figure 1: Illustration of the obtained FoS from the shear strength reduction method.

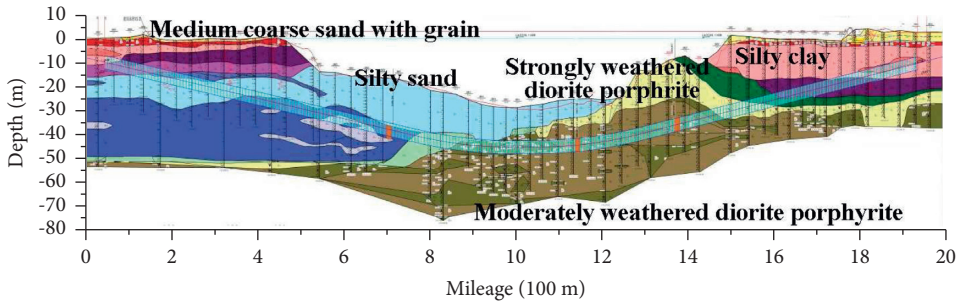

Figure 2: Geological profile of the river-crossing corridor.

are no much differences in the stratigraphic and hydrological conditions for those five opening points. As a result, there is only one numerical model created for the evaluation of the stability of the excavated weathered rock surface during the replacement of the cutter.

3.2.1. Model Parameters. Considering the boundary effect, tunnel size, and soil depth, the size is set as 42 m in length, 42 m in width, 52 m in depth for the entire model, 6.2 m in diameter, and 0.35 m in thickness for the tunnel segment, as illustrated in Figure 3. Under the boundary condition, the normal displacement is 0 and tangential displacement is free on the front, back, left, and right surfaces. The tangential and normal displacement are 0 on the bottom surface. Top surface is displacement free. All boundaries are permeable except the bottom surface, and the water level is globally consistent. The rock parameters E_m, ν, and γ used in the numerical simulation are determined from the soil investigation report GSK26, and m_i *GSI* and *D* are determined by rock type, texture, excavation method, structure, and surface condition following the recommendation from Manoj [17]. Rock and segment parameters are shown in Tables 1 and 2.

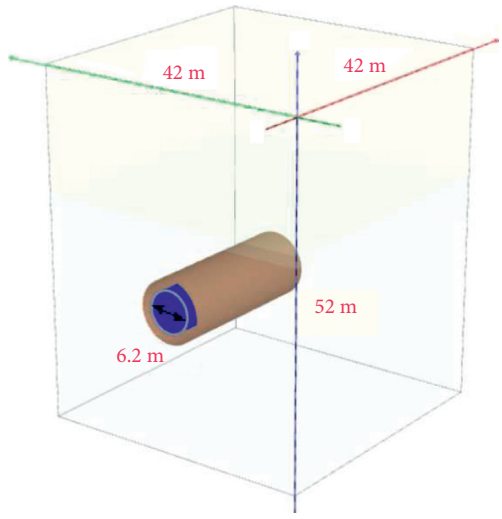

Figure 3: Numerical calculation model.

3.2.2. The Supporting Pressure on the Excavated Surface. The slurry is used to support the excavation face during excavation and the slurry level is maintained at the center of the excavation surface during the chamber opening process, as shown in Figure 4. The pressure generated by the slurry

Table 1: Rock parameters (Hoek–Brown model).

Types	Elastic modulus, E_m (MPa)	Poisson's ratio, ν	Uniaxial compressive strength, σ_c (MPa)	HB constant, m_i	Geological index strength, *GSI*	Disturbance parameter, *D*	Weight, γ (kN/m^3)
Strongly weathered diorite porphyrite	335	0.3	4	25	19	0	25.2
Moderately weathered diorite porphyrite	1628	0.3	33.39	25	28	0	26.3
Fractured diorite porphyrite	548	0.3	6	25	24	0	25.6

Table 2: Segment parameters (linear elastic model).

Type	Elastic modulus, *E* (MPa)	Poisson's ratio, ν	Weight, γ (kN/m^3)	Thickness, mm
Concrete	27600	0.2	6	350

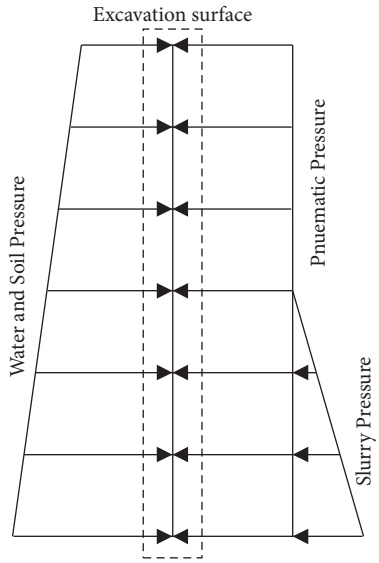

Figure 4: The support pressure.

can balance the Earth pressure on the excavation surface. To ensure the safe work environment for the TBM, it seems to be necessary to conduct the systematic study on the stability of the excavated surface during the chamber opening. The chamber opening can be divided into atmospheric opening and pressure support opening. Atmospheric opening has little influence on the entering staff, and it does not need to establish the mud film on the excavation surface; meanwhile, the construction period is shorter. Therefore, atmospheric opening should be preferred if it is available. When the stability of the excavation surface is insufficient, mud film should be established, and pressure support opening should be selected after having certain waterproof and air tightness. It is generally believed that the support pressure which is equal to the pressure of water and soil at the center of the tunnel is enough for support, but the upper limit value of the support pressure is set in practical project, so this paper discusses the stability of the excavation surface under a wide range of support pressure distribution. According to the water and soil partition algorithm, the pressure at the center of the tunnel at the first opening point in the actual project is 658 kPa. Based on this value, 0 kPa–1100 kPa in the simulation is generated every 100 kPa. The FoS of each working condition is calculated and its failure modes are observed.

3.3. The Comparison between Numerical Simulation Results and Measured Results. In this project, the precast lining ring is assembled by staggered joints, consisting of a capping block, two adjacent blocks, and three standard blocks. The displacements of tunnel arch bottom, vault settlement, and horizontal convergence are monitored on-site. Monitoring data began to stabilize on the 8th day after the completion of lining, so the monitoring results of the first 7 days were ignored in this paper. Both field measured data and numerical data are illustrated in Figure 5. It is observed that results from the numerical analyses agree well with the field measured data.

4. The Stability of the Excavated Surface

The stabilities of the excavated weathered rock surface are evaluated by considering different working conditions. The parametric studies on the effects of the parameters of the rock material on the computed FoS are also conducted in this section.

4.1. Stability of the Excavated Surface under Different Damage Modes. Choosing the suitable supporting pressure on the excavated surface is challenging in the tunnel excavation. The FoSs for the stability of the excavated surface are evaluated by considering different supporting pressures, such as Case 1 to Case 12, as shown in Table 3. Numerical simulation was carried out under different support pressures. The partial computed FoS for the cases by adopting different supporting pressures are illustrated in Figure 6. The soil displacement vector diagrams and the variation FoS with respect to different supporting pressures are illustrated in Figures 7 and 8, respectively.

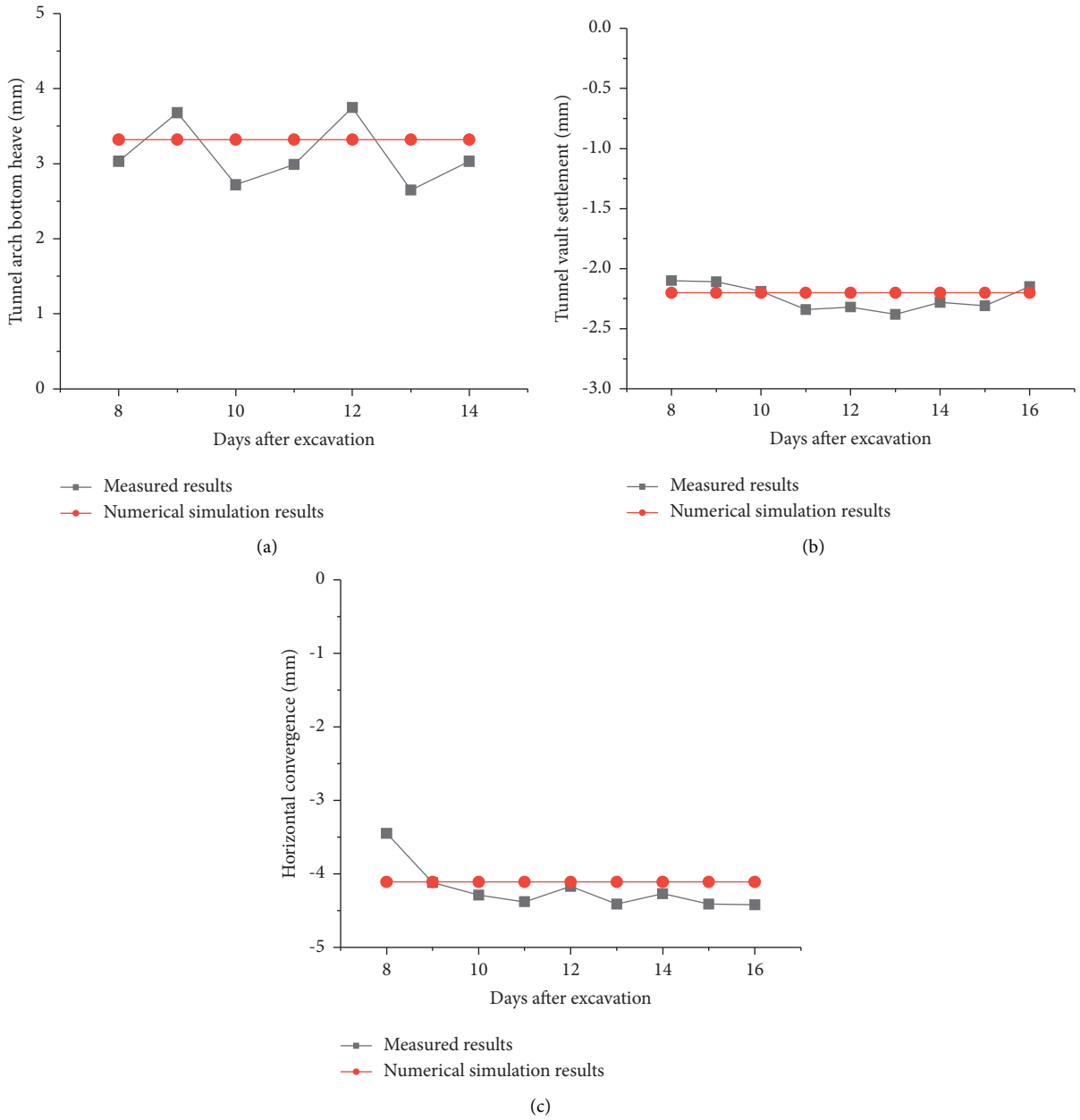

Figure 5: Comparison between monitoring results and numerical calculation results. (a) Tunnel arch bottom heave, (b) tunnel vault settlement, and (c) horizontal convergence.

Table 3: FoSs under different support pressures.

Case number	1	2	3	4	5	6	7	8	9	10	11	12
Support pressure (kPa)	0	100	200	300	400	500	600	700	800	900	1000	1100
FoS	2.88	3.54	3.54	4.10	5.07	5.77	7.70	10.91	14.04	17.25	13.08	9.87

It is observed that the minimum FoS is 2.89 under atmospheric pressure and the maximum FoS is 17.25 under supporting pressure of 900 kPa. The maximum horizontal Earth pressure at the center of excavated surface is 658 kPa calculated by the water and soil partition algorithm. It can be seen that much or little support pressure is not conducive to the stability of the surface, and the support pressure corresponding to the maximum safety factor is about 1.35 times the theoretical Earth pressure.

By observing the failure behavior of rock, the failure modes under different supporting pressures can be divided into the following four types: central intrusion type, bilateral

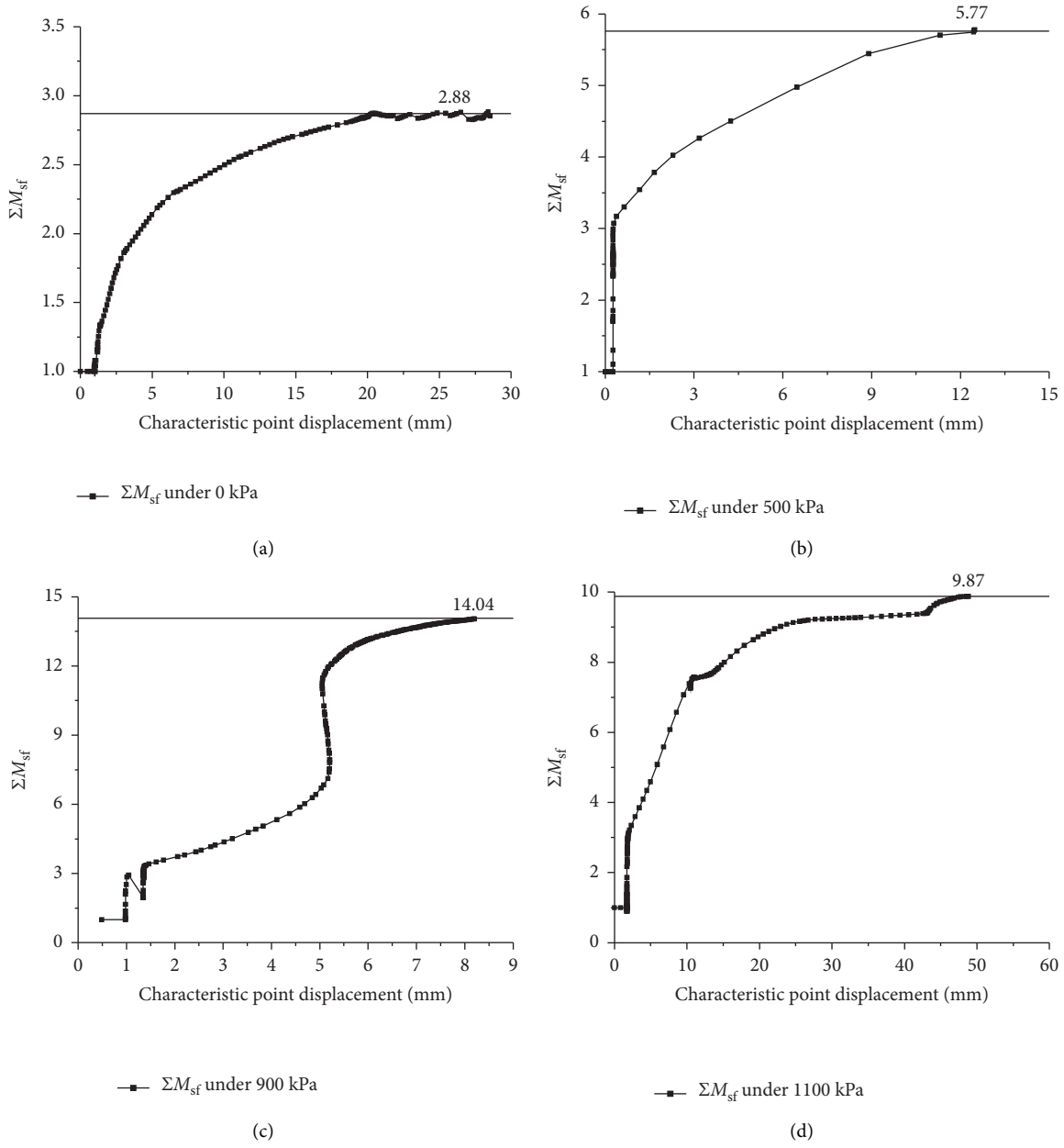

Figure 6: Safety factor curves under different pressure support. (a) 0 kPa (atmospheric pressure) (b) 500 kPa, (c) 900 kPa , and (d) 1100 kPa.

intrusion type, slipping type, and outward intrusion type. The center intrusion type refers to that the rock near the center of the tunnel will first have large deformation and invade the tunnel and collapse under the condition of small support pressure or atmospheric pressure. The bilateral intrusion type refers to that, under the support of slightly smaller pressure, the two sides of the horizontal line in the center of the tunnel will be destroyed first, invading into the tunnel and causing collapse. Slipping type refers to that, under the appropriate pressure support, the strength of rock is greatly reduced and shows fluid characteristics, sliding down along the surface under the action of gravity. The safety factor of slipping failure is high. The outward intrusion type refers to that, under the larger support pressure, the rock begins to shift away from the tunnel, and the safety factor decreases significantly. At the same time, excessive pressure may have an adverse effect on the mud film and cause the surface uplift in the front of the tunnel, which should be avoided as much as possible.

Under different supporting pressures, the bilateral intrusion type accounted for a large proportion; from 100 kPa to 600 kPa, all belong to this type. The mechanism of this failure, however, is puzzling. Bilateral intrusion type and center intrusion type show that rock intrudes into the tunnel, indicating that the support pressure is less than water and soil pressure. Under the action of two pressure differences, it seems that the rock near the center should be the first to produce the failure. However, with the increase of

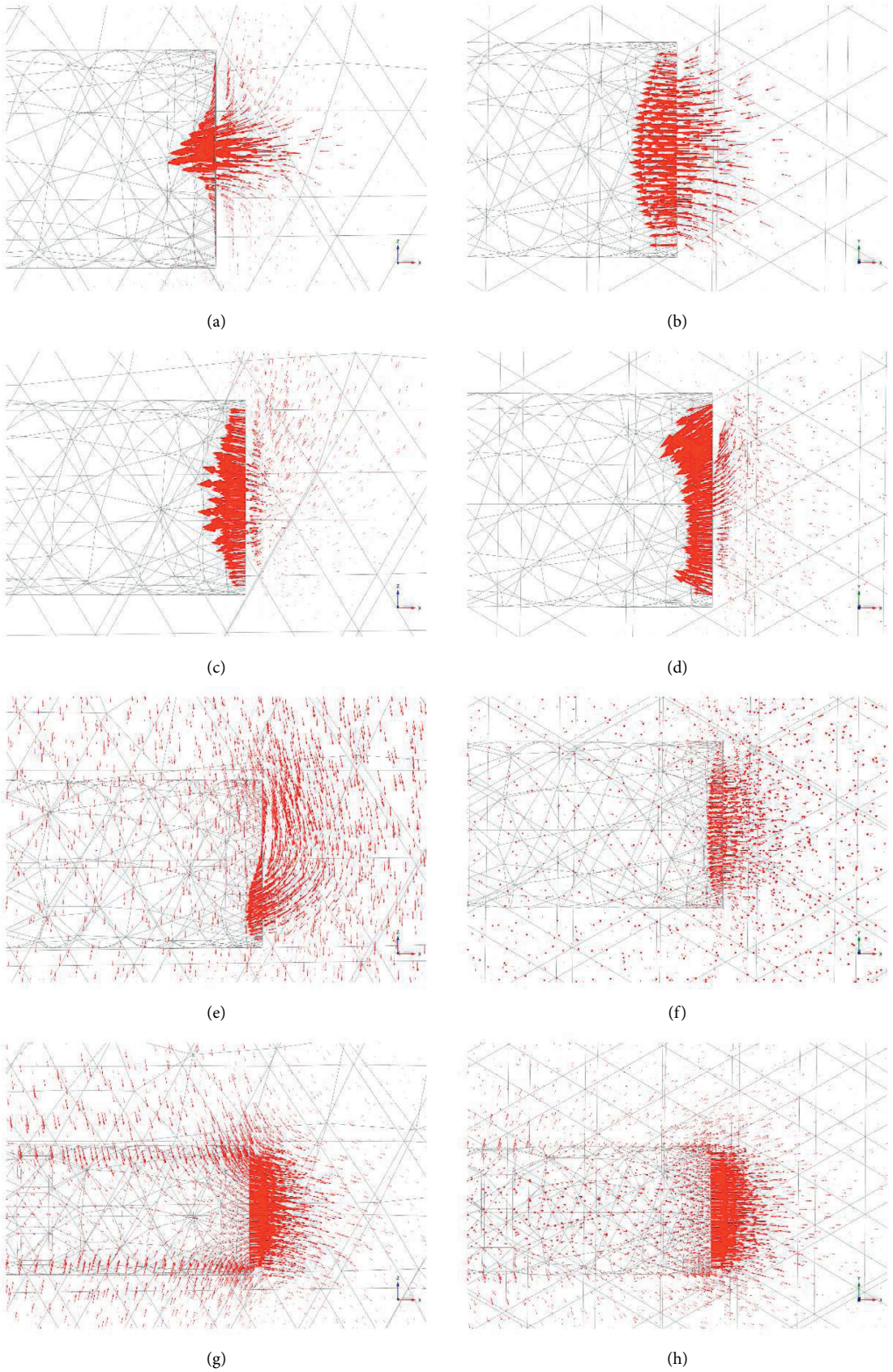

Figure 7: Soil displacement vector diagrams under different failure modes. (a) Lateral view of central intrusion. (b) Top view of central intrusion. (c) Lateral view of bilateral intrusion. (d) Top view of bilateral intrusion. (e) Lateral view of slip. (f) Top view of slip. (g) Lateral view of outward intrusion. (h) Top view of outward intrusion.

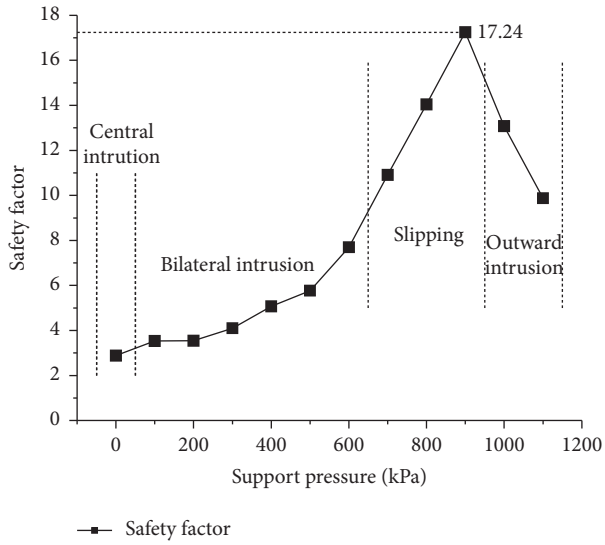

Figure 8: Relation curve between safety factor and support pressure.

support pressure, there is the bilateral intrusion. This paper considers that the occurrence of this failure mode may be related to the deformation of tunnel segment in numerical simulation. Under the action of rock pressure, the tunnel segment expands horizontally, and this deformation may affect the rock on both sides, making it more inclined to be the first to fail under the small difference between internal and external pressure. However, in fact, the cutter head does not deform like the segment, so the bilateral intrusion type may not be real.

4.2. Influence of Rock Parameters on FoS. Parametric analyses were conducted to investigate the effect of the parameters of rock mass on the computed FoS for the stability of excavated surface. The gray correlation method is a gray system analysis method [18], which can be used for the quantification of effect of the variation of the factor on the target variable. Therefore, the gray correlation method is used to analyze the effects of the variation in ν, σ_c, m_i, *GSI*, and D on the computed FoS. The analysis procedure using the gray correlation method is illustrated as follows.

4.2.1. Comparison Matrix and Reference Sequence. The comparison matrix $X_i(k)$ is composed of various influence factors, which is divided into 21 rows and 5 columns, representing 21 sets of values of 5 rock parameters within a reasonable range. The reference sequence $Y(k)$ consists of the target variable, including 21 excavation surface safety factors corresponding to the comparison matrix:

$$X_i(k) = \begin{bmatrix} X_1(1) & \dots & X_5(1) \\ \dots & & \\ X_1(21) & \dots & X_5(21) \end{bmatrix}, \quad Y(k) = \begin{bmatrix} Y(1) & \dots & Y(21) \end{bmatrix}^T. \tag{7}$$

4.2.2. Dimensionless Variables. Due to the different dimensions of each factor, it is not convenient for direct analysis. Therefore, in order to ensure the accuracy and reliability of the calculation results, it is necessary to carry out the dimensionless treatment of each variable and obtain the new comparison matrix $X'_i(k)$ and the reference sequence $Y'(k)$:

$$X'_i(k) = \frac{X_i(k) - X_{\min}}{X_{\max} - X_{\min}}, \quad Y'(k) = \frac{Y(k) - Y_{\min}}{Y_{\max} - Y_{\min}}. \tag{8}$$

4.2.3. Correlation Matrix. Using the above dimensionless calculation results, a new difference sequence matrix Δ is calculated. According to Δ, the correlation coefficient matrix ω can be constructed as equation (10):

$$\Delta_{ij} = \left| X'_i(k) - Y'(k) \right|, \tag{9}$$

$$\omega_{ij} = \frac{\Delta_{\min} + \rho\Delta_{\max}}{\Delta_{ij} + \rho\Delta_{\max}}, \tag{10}$$

where $\Delta_{max} = \max\Delta_{ij}$, $\Delta_{min} = \min\Delta_{ij}$, and ρ is the resolution factor, which can be used to adjust the resolution of each influence factor, and the value range is (0, 1) typically taken as 0.5 [19].

4.2.4. Correlation Degree. Correlation degree ξ_i is the quantitative description of the degree of influence between the influence factors and the target variables, $0 \leqq \xi_i \leqq 1$, the greater the value is, the stronger the association is:

$$\xi_i = \frac{1}{n} \sum_{1}^{n} \omega_{ij}. \tag{11}$$

After the above calculation process, the correlation degree of each factor is shown in Figure 9.

The obtained correlation degree between factors (including σ_c, ν, m_i, *GSI*, and D) and computed FoS is illustrated in Figure 9. It can be seen that, among those five factors, σ_c and *GSI* have significant effect on the computed FoS, followed by D and ν. It is observed that m_i has least significant effect on computed FoS. Based on the Hoek–Brown failure criterion, the shear strength of rock is mainly governed by σ_c and *GSI*. Meanwhile, the variation range of parameters will also affect the uncertainty of the analyzed results. It is observed from the technical report and the manual of the commercial software; the variation of parameters ν, m_i, and D is commonly small. As a result, the effects of the variations of σ_c and *GSI* on the computed FoS are investigated and illustrated in Figure 10.

Figure 10 indicates that FoS increases with increase in σ_c or *GSI*. It seems there is a linear relationship between the computed FoS and *GSI*, while there is hyperbolic relationship between FoS and σ_c. According to the soil investigation report, the average value of σ_c in moderately weathered rock

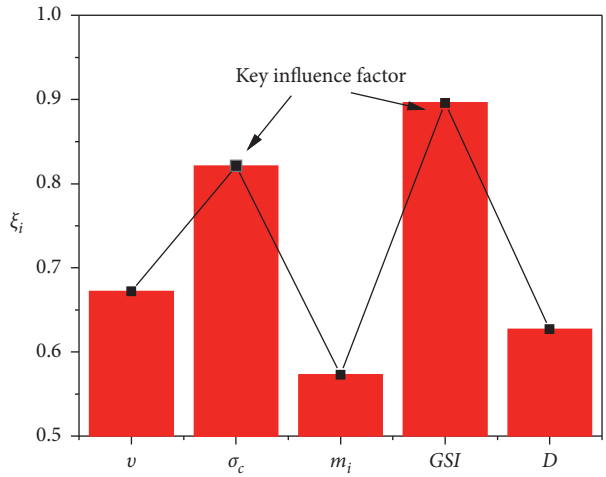

FIGURE 9: Correlation degree between influence factors and FoS.

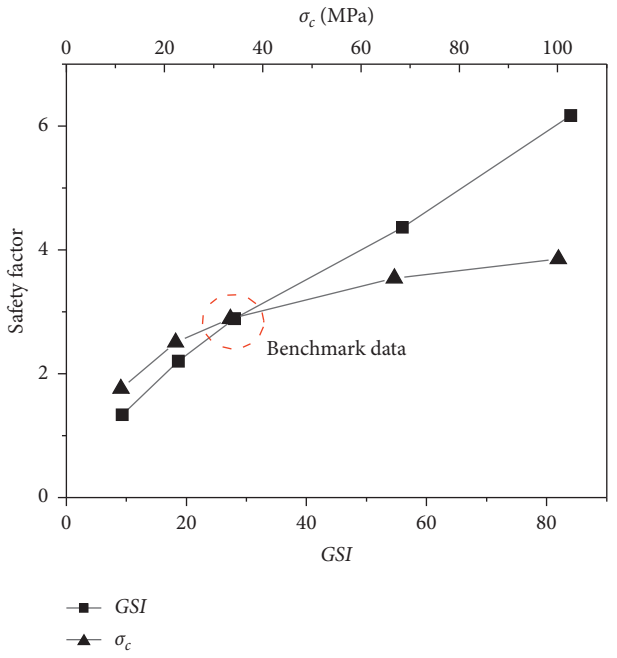

FIGURE 10: Illustration of FoS with respect to the variation of σ_c and *GSI*.

is 34.11 MPa, the standard value is 31.19 MPa, and the rock is relatively complete. According to the engineering manual of PLAXIS 3D, *GSI* can be taken as 60–70. Therefore, the excavated surface is still stable by considering the spatial variability of key geotechnical parameters of rock.

5. Conclusions

The computed displacements of tunnel arch bottom, vault settlement, and horizontal convergence agree well with the field measured data. The FoSs for the excavated weathered rock surface by considering different supporting pressure are computed. Based on the analyzed result, rock failure mode can be divided into four types: central intrusion type, bilateral intrusion type, slipping type, and outward intrusion type. The parametric study on the parameters of rock on the computed FoS is also conducted. It is observed that σ_c or *GSI* have significant effect on the computed FoS, while m_i has least significant effect on FoS.

Data Availability

All data and models generated or used during the study are included within the article.

Conflicts of Interest

The authors declare that they have no conflicts of interest.

Acknowledgments

The last three authors would like to acknowledge the financial support they received from the National Natural Science Foundation of China (nos. 51878160 and 52078128) and China Huaneng Group Co. Ltd. (no. HNKJ19-H17).

References

[1] D. G. Fredlund and M. D. Fredlund, "Keynote Lecture: Developments in Landslide Analysis," in *Proceedings of the paper presented at the 4th International Conference on Geotechnics for Sustainable Infrastructure Development (GEOTEC HANOI)*, Hanoi, VIETNAM, November 2019.

[2] D. V. Griffiths and P. A. Lane, "Slope stability analysis by finite elements," *Géotechnique*, vol. 49, no. 3, pp. 387–403, 1999.

[3] A. P. Dyson and A. Tolooiyan, "Optimisation of strength reduction finite element method codes for slope stability analysis," *Innovative Infrastructure Solutions*, vol. 3, no. 1, 2018.

[4] P. Li, H. Liu, and Y. Zhang, "Based on the Strength Reduction Slope Stability Finite Element Analysis of Engineering Examples," in *Proceedings of the 2nd International Conference on Civil Engineering, Architecture and Building Materials (CEABM 2012)*, vol. 170-173, Yantai, China, 2012 May.

[5] X. Lü, Z. Su, M. Huang, and Y. Zhou, "Strength reduction finite element analysis of a stability of large cross-river shield tunnel face with seepage," *European Journal of Environmental and Civil Engineering*, vol. 24, no. 3, pp. 336–353, 2020.

[6] C. Shi, X. Feng, and Q. Jiang, "Calculation of underground tunnels' safety factor based on the strength reduction technique," *Advanced Materials Research* in *Proceedings of the Global Conference on Civil, Structural and Environmental Engineering/3rd International Symp on Multi-Field Coupling Theory of Rock and Soil Media and its Applications*, vol. 594-597, Yichang, China, 2012 October.

[7] W. Fu and Y. Liao, "Non-linear shear strength reduction technique in slope stability calculation," *Computers and Geotechnics*, vol. 37, no. 3, pp. 288–298, 2010.

[8] G. You, M. Al Mandalawi, A. Soliman, K. Dowling, and P. Dahlhaus, "Finite Element Analysis of Rock Slope Stability Using Shear Strength Reduction Method," in *Proceedings of the International Congress and Exhibition on Sustainable Civil Infrastructures*, Sharm El Sheikh, EGYPT, July 2017.

[9] H. Van Langen and P. A. Vermeer, "Automatic step size correction for non-associated plasticity problems," *International Journal for Numerical Methods in Engineering*, vol. 29, no. 3, pp. 579–598, 1990.

[10] R. B. J. Brinkgreve and H. L. Bakker, "NONLINEAR FINITE-ELEMENT ANALYSIS OF SAFETY FACTORS," in *Proceedings of the paper presented at the 7th International Conf on Computer Methods and Advances in Geomechanics*, Cairns, Australia, May 1991.

[11] R. E. Hammah, T. Yacoub, B. Corkum, and J. Curran, "The shear strength reduction method for the generalized Hoek-Brown criterion," in *Proceedings of the 40th US Symposium on Rock Mechanics*, Anchorage, Alaska, January 2005.

[12] T. Benz, R. Schwab, R. A. Kauther, and P. A. Vermeer, "A Hoek-Brown criterion with intrinsic material strength factorization," *International Journal of Rock Mechanics and Mining Sciences*, vol. 45, no. 2, pp. 210–222, 2008.

[13] A. J. Li, R. S. Merifield, and A. V. Lyamin, "Effect of rock mass disturbance on the stability of rock slopes using the Hoek-Brown failure criterion," *Computers and Geotechnics*, vol. 38, no. 4, pp. 546–558, 2011.

[14] J. Shen, M. Karakus, and C. Xu, "Chart-based slope stability assessment using the Generalized Hoek-Brown criterion," *International Journal of Rock Mechanics and Mining Sciences*, vol. 64, pp. 210–219, 2013.

[15] E. Hoek and E. T. Brown, "Empirical strength criterion for rock masses," *Journal of the Geotechnical Engineering Division*, vol. 106, no. 9, pp. 1013–1035, 1980.

[16] E. Hoek, C. C-T, and B. Corkum, "Hoek-Brown Failure Criterion—2002 Edition," in *Proceedings of the 5th North American symposium—NARMS-TAC*, Toronto, Canada, January 2002.

[17] R. B. J. B. L. M. Z. N. R. Manoj, *PLAXIS CONNECT Edition V20*, PLAXIS company, Netherlands, 2019.

[18] B. Li, J. Wei, and R. Bian, "A Dynamic Three-Dimensional Correlation Space Model for Multi-Attribute Decision Problems," in *Proceedings of the 2015 IEEE International Conference on Grey Systems and Intelligent Services (GSIS)*, Leicester, UK, August 2015.

[19] J. Tu and A. Tang, "A Grey Correlation Model for Analyzing Ultimate Bearing Capacity of Large Diameter and Super-long Pile," in *Proceedings of the International Conference on Applied Mechanics and Mechanical Engineering (ICAMME 2011)*, Sanya, China, October 2011.